Supporting Information

Multifunctional Waste Biomass-Derived Solar Evaporator for Efficient and Sustainable Solar-Driven Clean Water Evaporation

Hongbin Cao,[a] Haiyan Wang,[a] Xiu He,[b] Yuxin Yang,[c,*] Tongyan Ren,[a] Lvhua Liu,[a] Yanyan Zheng,[a] Jingjing Fu,[a,*] Huang Zhou,[a,*]

[a] Department of Chemistry, School of Pharmacy and Institute of Pharmacy, North Sichuan Medical College, Nanchong 637100, P. R. China

[b] Department of Cell Biology and Genetics Chemistry, School of Basic Medical Sciences and Forensic Medicine, North Sichuan Medical College, Nanchong 637100, P. R. China

[c] School of Mechanical Engineering, Chengdu University, Chengdu 610000, P. R. China

***Corresponding author:** Prof. Huang Zhou; Dr. Jingjing Fu; Prof. Yuxin Yang

E-mail: zhouhuangcbyxy@163.com; fujingjing1991@nsmc.edu.cn; yangyuxin@cdu.edu.cn

Number of pages: 24

Number of figures: 16

Note S1.

The water evaporation rate reflects the mass flux due to evaporation of water, which is defined by Equation 1

$$\bar{m} = \frac{\Delta m}{S \cdot t} \quad (1)$$

where Δm is the mass change due to the water evaporation (kg), S is the solar irradiation area (m^2), and t is the irradiation time (h). To account for natural evaporation that occurs in the absence of light, the evaporation rate should be determined as the difference between the rates under light and dark conditions ($\bar{m} = \bar{m}_{light} - \bar{m}_{dark}$). [R1, R2]

The solar thermal conversion efficiency (η) can be expressed by eq2 [R3, R4]

$$\eta = \frac{\bar{m} \cdot h_{LV}}{C_{opt} \cdot P_0} \quad (2)$$

where C_{opt} is the optical concentration and P_0 is the solar power intensity of 1 sun; $h_{LV} = C \cdot \Delta T + h_{vap}$ is the total enthalpy change, which is the sum of sensible enthalpy for temperature rise and phase change enthalpy, C is the specific heat capacity (~4.2 J g^{-1} $°C^{-1}$) of water. ΔT is the temperature difference between membrane (T_1) and water (T_2), and h_{vap} is the enthalpy of vaporization (2257.6 kJ kg^{-1}).

[R1] Finnerty, C.; Zhang, L.; Sedlak, D. L.; Nelson, K. L.; Mi, B. Synthetic Graphene Oxide Leaf for Solar Desalination with Zero Liquid Discharge. *Environ. Sci. Technol.* **2017**, *51*, 11701-11709.

[R2] Zhou, J.; Gu, Y.; Liu, P.; Wang, P.; Miao, L.; Liu, J.; Wei, A.; Mu, X.; Li, J.; Zhu, J. Development and Evolution of the System Structure for Highly Efficient Solar Steam Generation from Zero to Three Dimensions. *Adv. Funct. Mater.* **2019**, *29*, 1903255.

[R3] Kuang, Y.; Chen, C.; He, S.; Hitz, E. M.; Wang, Y.; Gan, W.; Mi, R.; Hu, L. A High-Performance Self-Regenerating Solar Evaporator for Continuous Water Desalination. Adv. Mater. 2019, 31, 1900498.

[R4] Liu, P.-F.; Miao, L.; Deng, Z.; Zhou, J.; Gu, Y.; Chen, S.; Cai, H.; Sun, L.; Tanemura, S. Flame-Treated and Fast-Assembled Foam System for Direct Solar Steam Generation and Non-Plugging High Salinity Desalination with Self-Cleaning Effect. *Appl. Energy* **2019**, *241*, 652-659.

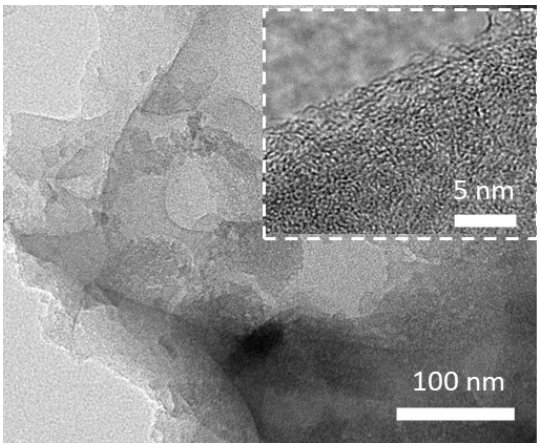

Fig. S1 – The TEM image of the VRC.

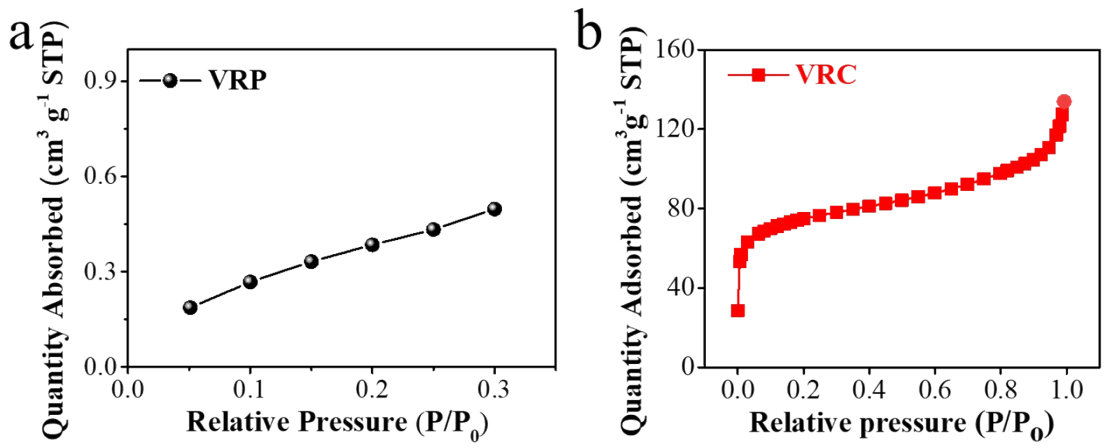

Fig. S2 – N_2 adsorption isotherm of the (a) VRP and (b) VRC.

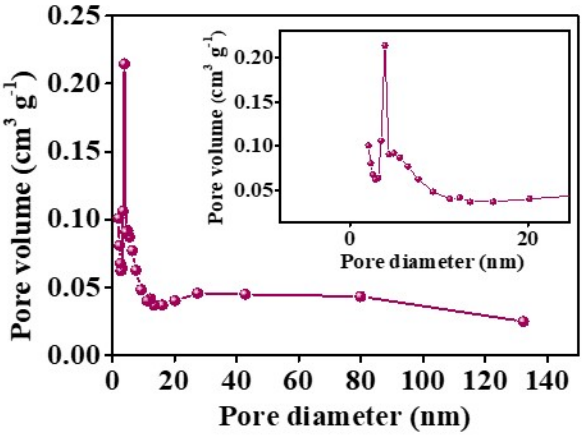

Fig. S3 – The pore distribution curve and mesopore ratio of VRC.

Note S2.

During activation, KOH can react with the carbon in the PAC as follows:

$$6KOH + 2C \longrightarrow 2\,K + 3H2 + 2K_2CO_3 \quad (1)$$

When the activation temperature exceeded 500 ℃, the reaction (2) can occur. [R1]

$$K_2CO_3 \longrightarrow K_2O + CO_2 \quad (2)$$

The pore development was generally ascribable to (1) the oxidation of carbon to carbonate, (2) activation with CO_2 from K_2CO_3 decomposition, and potassium metal intercalation between the carbon lattices.

[R1] Li, D.; Tian, Y.; Li, L.; Li, J.; Zhang H. Production of Highly Microporous Carbons with Large CO_2 uptakes at Atmospheric Pressure by KOH Activation of Peanut Shell Char. *J. Porous. Mater*. **2015**, *22*, 1581-1588.

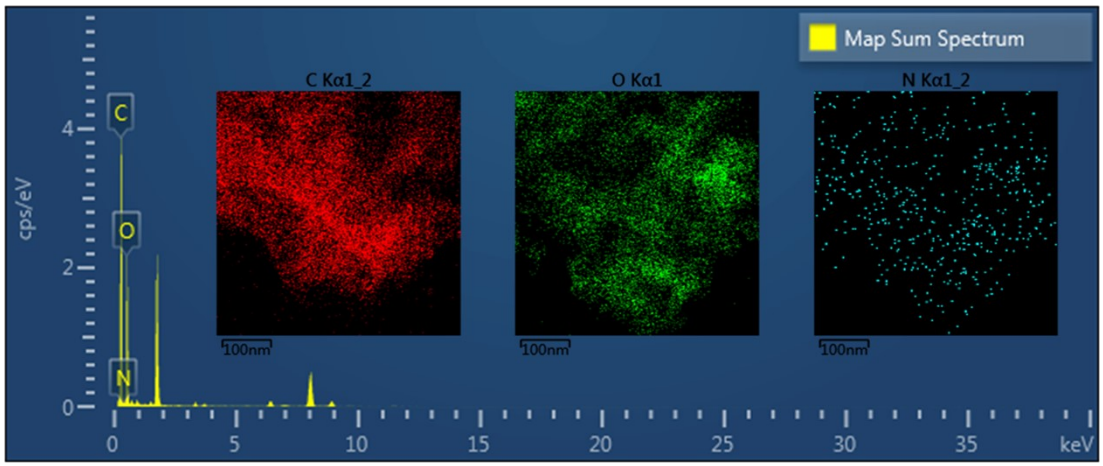

Fig. S4 – EDX elemental mapping of C, O and N elements for the same piece of the VRC.

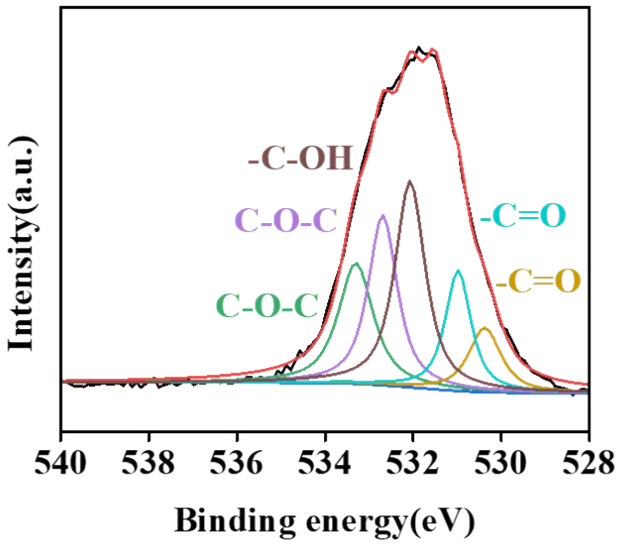

Fig. S5 – XPS results of the obtained VRC of O 1s.

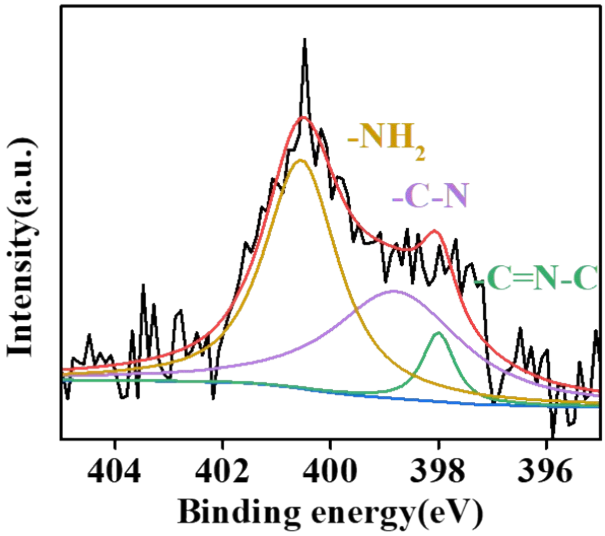

Fig. S6 – XPS results of the obtained VRC of pyridinic N, pyrrolic N and graphitic N bindings.

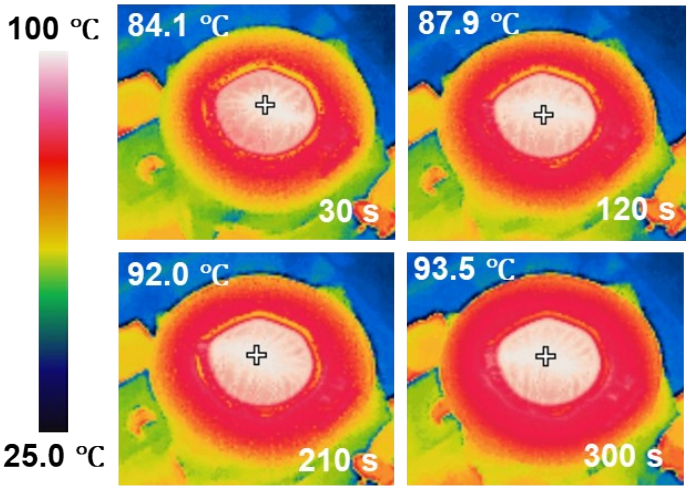

Fig. S7 – Top view thermal image of the MWBP evaporator after sunlight illumination for 300 s.

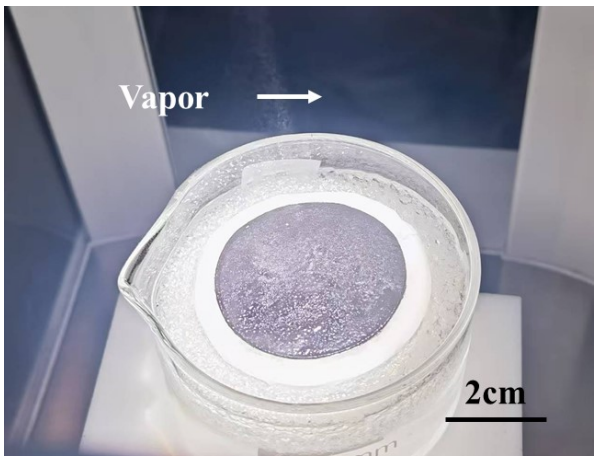

Fig. S8 – The rapid evaporation of seawater was observed by the naked eye.

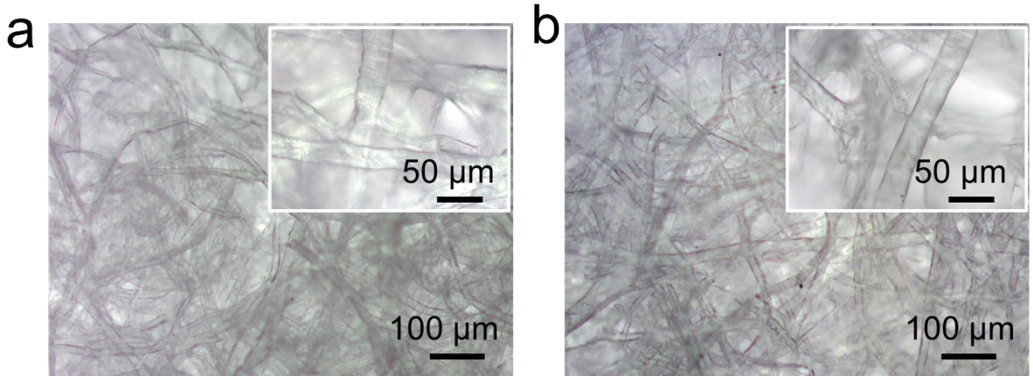

Fig. S9 – The morphology of the filter paper (a) before and (b) after working 6 months.

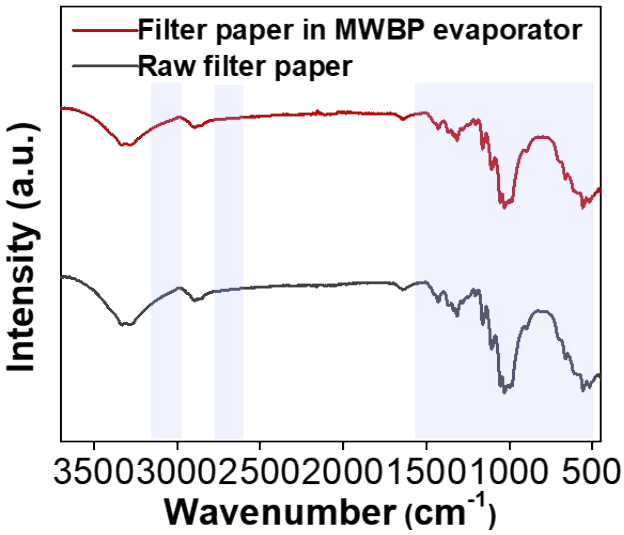

Fig. S10 – The FTIR of the filter paper (a) before and (b) after working 6 months.

Note S3.

The thermal-insulating reduced heat loss of the whole evaporation including 1) radiation loss P_{rad}, 2) convection loss P_{conv} and 3) conduction loss P_{cond}, detailed thermal loss analysis was performed as following calculations.

1) The radiation flux P_{rad} can be calculated by Stefan-Boltzmann law.

$$P_{rad} = \varepsilon\sigma (T_1^4 - T_2^4) \quad \text{(S1)}$$

Where ε is the emissive rate (0.93), σ is the Stefan-Boltzmann constant (assumed to be 5.67×10^{-8} W $(m^2 \cdot K^4)^{-1}$), T_1 (321.6 K) is the surface temperature of absorber at steady state under 1 sun illumination, and T_2 (319.1 K) is the ambient temperature upward the absorber under 1 sun illumination. The top surface of the absorber is surrounded by heated vapor, which is very close to the temperature of MWBP evaporator surface, the radiative and convective loss should be very small. As a result, the radiation heat flux is estimated to be 19 W/m^2, the radiation loss is about 1.9 %.

2) The convection loss P_{conv} can be calculated by Newton's law of cooling.

$$P_{conv} = h (T_1 - T_2) \quad \text{(S2)}$$

where P_{conv} denotes convection heat flux, h is the convection heat transfer coefficient (10 W $(m^2 K)^{-1}$). Here, the convection heat is estimated as ≈ 25 W/m^2, and the radiation loss is about 2.5 %.

3) Conduction loss P_{cond} is based on Fourier's law.

$$P_{cond} = (A'/A)\, q_{water} \quad \text{(S3)}$$

$$q_{water} = \kappa(\Delta T/\Delta L) \quad \text{(S4)}$$

Where the A' is the direct contact area between water and evaporator, the q_{water} is the heat flux transferred to water. With the occupation of water, the thermal

conductivity κ is closed to water (0.599 $W/m \cdot K^{-1}$), the $\triangle T/\triangle L$ is approximate 40 K/m and A'/A was estimated to be 0.40. Thus, the conductive loss is about 9.6 W/m^2 and the heat loss rate is about 1.0 %.

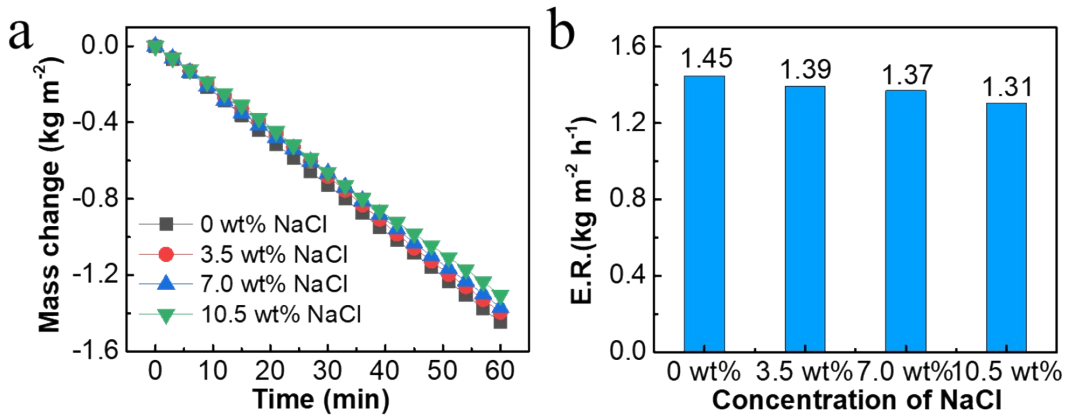

Fig. S11 – The evaporation performance of the MWBP evaporator is illustrated through (a) the mass change and (b) ERs variations across 0-10.5 wt% NaCl brine concentrations under 1 sun irradiation.

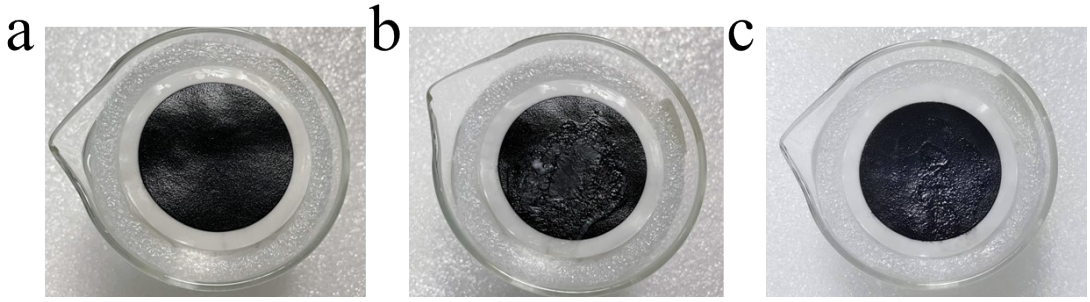

Fig. S12 – The salt rejection test of the MWBP evaporator. (a) The initial image of the MWBP evaporator. (b) The image of the MWBP evaporator after 10 h solar evaporation. (c) The self-desalting performance of MWBP evaporator in the dark overnight.

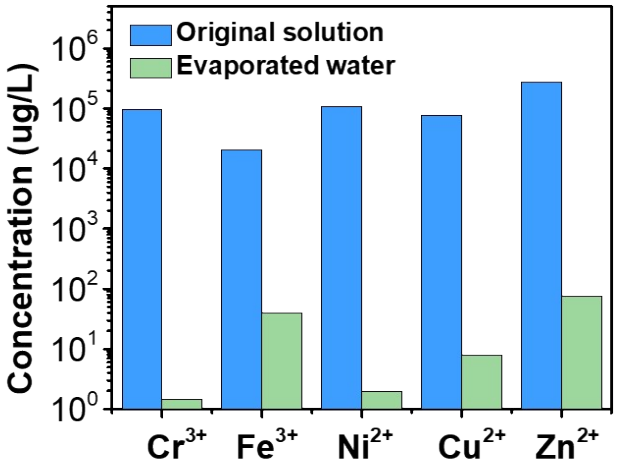

Fig. S13 – The concentrations of the heavy metal cations before and after desalination.

Table R1. Comparison of the antibacterial properties, cost-effectiveness, cycling stability and energy conversion efficiency of MWBP evaporator with other reported biomass-based evaporators under solar illumination of 1 kW m^{-2}.

Biomass-derived evaporators	Efficiency (%)	Cost ($/g)	Cycling stability	Antibacterial properties	Ref
Wood	76%	0.55	20	–	[1]
Loofah sponge	89.9	0.0055	–	–	[2]
Green Moss	83%	0.0094	–	–	[3]
Coconut husk	90.2%	0.0040	10	–	[4]
Reed straw	87.8%	0.0043	10	–	[5]
Sugarcane	77.3%	0.0032	20	–	[6]
Banana peel	87.5%	0.0020	15	–	[7]
Loofah	83.7%	0.460	10	–	[8]
Lophius litulon	90.6%	0.02	–	–	[9]
Enteromorpha prolifera	84%	0.0074	–	–	[10]
Lignin	72.5%	0.0037	7	–	[11]
K-wood	81.4	0.50	20	–	[12]
Vinager residue	91.5%	0.0019	15	**Yes**	**This work**

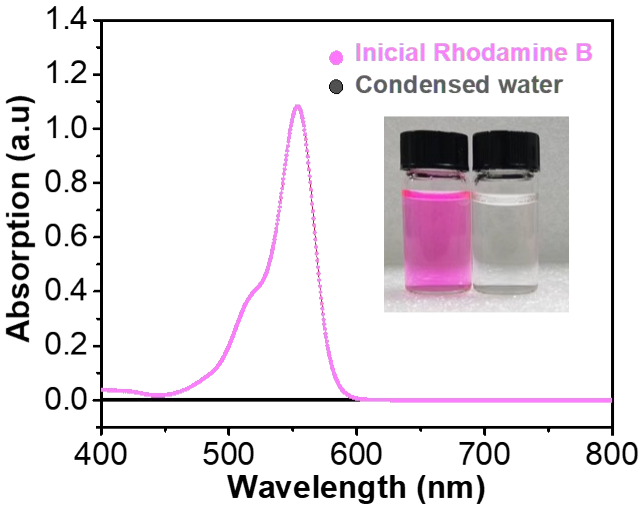

Fig. S14 – The UV-Vis absorption spectra and photographs of RB-polluted water before and after solar evaporation.

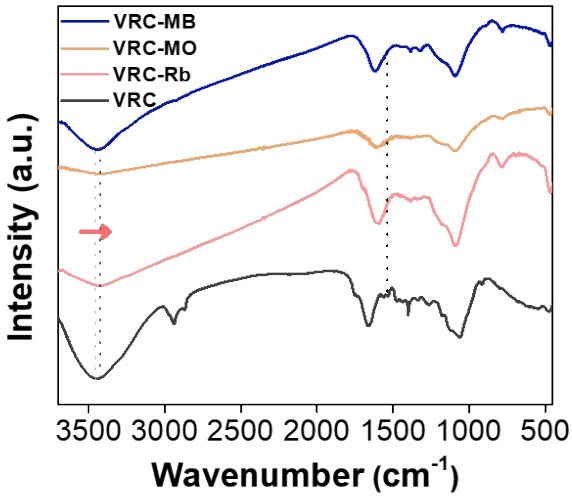

Fig. S15 – The FT-IR spectroscopic analysis was conducted on VRC samples before and after pollutant adsorption.

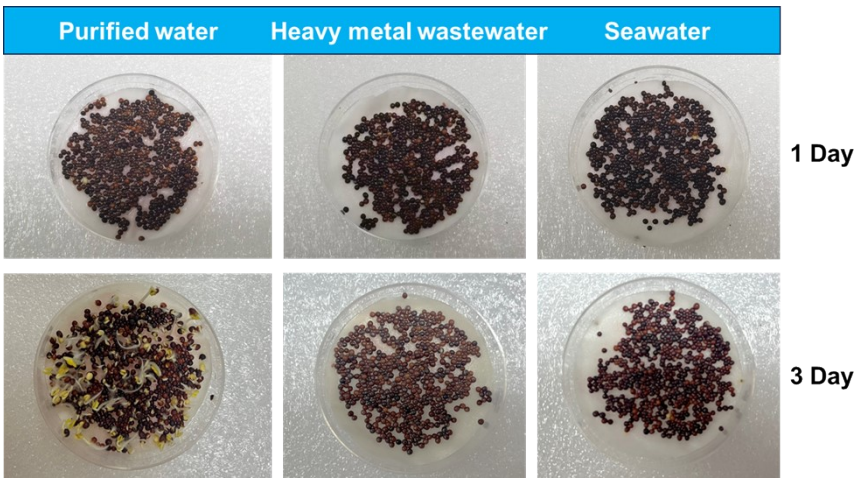

Fig. S16 – Pictures of cabbage seed germination using different water samples.

References

[1] Z. Yu, S. Cheng, C. Li, Y. Sun, B. Li, Enhancing efficiency of carbonized wood based solar steam generator for wastewater treatment by optimizing the thickness, Sol. Energy, 2019, 193, 434–441.

[2] C. Liu, K. Hong, X. Sun, A. Natan, P. Luan, Y. Yang, H. Zhu, An 'antifouling' porous loofah sponge with internal microchannels as solar absorbers and water pumpers for thermal desalination, J. Mater. Chem. A, 2020, 8, 12323–12333.

[3] J. Li, X. Zhou, J. Zhang, C. Liu, F. Wang, Y. Zhao, H. Sun, Z. Zhu, W. Liang, A. Li, Migration crystallization device based on biomass photothermal materials for efficient salt-rejection solar steam generation, ACS Appl. Energ. Mater. 2020, 3, 3024–3032.

[4] J. Li, X. Zhou, G. Chen, F. Wang, J. Mao, Y. Long, H. Sun, Z. Zhu, W. Liang, A. Li, Evaporation efficiency monitoring device based on biomass photothermal material for salt-resistant solar-driven interfacial evaporation, Sol. Energy Mater. Sol. Cells, 2021, 222, 110941.

[5] J. Liu, L. Xu, Y. Li, J. Zhao, X. Jia, J. Chao, B. Lv, Y. Zhao, Construction of novel biomass-based solar evaporator with asymmetric dual-layer structure for water desalination, Adv. Sustain. Syst. 2021, 6, 2100274.

[6] J. Xiong, Z. Zhang, Y. Liu, J. Yi, Y. Wang, B. Li, W. Wang, S. Peng, X. Min, Y. Gui, M. Li, J. Peng, Full bagasse bio-waste derived 3D photothermal aerogels for high efficient solar steam generation, Cellulose, 2021, 29, 927–939.

[7] S. Ma, Q. Wang, K. Chen, W. Yuan, X. Gao, N. Li, N. Gao, Biomass waste-derived

solar evaporator for efficient and low-cost water evaporation, Energ. Technol. 2022, 10, 2200900.

[8] Y. Lu, X. Wang, D. Fan, H. Yang, H. Xu, H. Min, X. Yang, Biomass derived Janus solar evaporator for synergic water evaporation and purification, Sustain. Mater. Techno. 2020, 25, e00180.

[9] J. Wang, Z. Zhao, C. Yang, M. Sun, J. Chen, Y. Zhou, H. Xu, Marine biomass metal-organic framework hybrid evaporators for efficient solar water purification, Desalination, 2023, 556, 116577.

[10] L. Yang, G. Chen, N. Zhang, Y. Xu, X. Xu, Sustainable biochar-based solar absorbers for high-performance solar-driven steam generation and water purification, ACS Sustain, Chem. Eng. 2019, 7, 19311–19320.

[11] Z. Wang, Y. Yan, X. Shen, C. Jin, Q. Sun, H. Li, A wood–polypyrrole composite as a photothermal conversion device for solar evaporation enhancement, J. Mater. Chem. A, 2019, 7, 20706–20712.

[12] D. Li, D. Han, C. Guo, C. Huang, Facile preparation of MnO_2-deposited wood for high-efficiency solar steam generation, ACS Appl. Energ. Mater. 2021, 4, 1752–1762.